FISEVIER

Contents lists available at ScienceDirect

# Colloids and Surfaces B: Biointerfaces

journal homepage: www.elsevier.com/locate/colsurfb



# Zn<sup>2+</sup>-assisted photothermal therapy for rapid bacteria-killing using biodegradable humic acid encapsulated MOFs



Ziwei Liu<sup>a</sup>, Lei Tan<sup>a</sup>, Xiangmei Liu<sup>a</sup>,\*, Yanqin Liang<sup>b</sup>, Yufeng Zheng<sup>c</sup>, Kelvin Wai Kwok Yeung<sup>d</sup>, Zhenduo Cui<sup>b</sup>, Shengli Zhu<sup>b</sup>, Zhaoyang Li<sup>b</sup>, Shuilin Wu<sup>b</sup>,\*

- <sup>a</sup> Hubei Key Laboratory of Polymer Materials, School of Materials Science & Engineering, Ministry-of-Education Key Laboratory for the Green Preparation and Application of Functional Materials, Hubei University, Wuhan, 430062, China
- b The Key Laboratory of Advanced Ceramics and Machining Technology by the Ministry of Education of China, School of Materials Science & Engineering, Tianjin University, Tianjin, 300072, China
- <sup>c</sup> State Key Laboratory for Turbulence and Complex System, Department of Materials Science and Engineering, College of Engineering, Peking University, Beijing, 100871, China

#### ARTICLE INFO

#### Keywords: Humic acid MOF Photothermal Controlled release Antibacterial

#### ABSTRACT

Bacterial infection is seriously threatening human health all over the world, especially with the emergence of increasing drug-fast bacteria. It is urgent to develop a drug-free strategy to kill bacteria rapidly and efficiently. In this work, humic acid (HuA) encapsulated zeolitic imidazole framework-8 (ZIF-8) (HuA@ZIF-8) nanocomposites are synthesized by the *in-situ* growth of ZIF-8 on the surface of polyvinylpyrrolidone (PVP)-modified HuA. The synthesized nanocomposites possesses good photothermal effects, *i.e.*, the temperature increased to 59.4 °C under the particle concentration of 1000  $\mu$ g/mL with 10 min NIR irradiation. In addition, NIR irradiation can also control the release of Zn<sup>2+</sup> from the composites. The good photothermal effects originate from HuA that can effectively absorb NIR light. The controlled release of Zn<sup>2+</sup> is ascribed to the induced-dissociation of ZIF-8 under NIR light irradiation. The synergistic action of photothermal therapy and release of zinc ions contributes to the excellent antibacterial efficiency of HuA@ZIF-8 within a short time, *i.e.* 99.59 % and 99.37 % against *Staphylococcus aureus* and *Escherichia coli* with 20 min NIR irradiation, respectively. This work provides a promising strategy to develop a light-responsive platform with good biodegradability and low cost for rapid and effective sterilization.

### 1. Introduction

Pathogenic bacteria are one of the most common causes of human diseases and can induce deadly infections [1–3]. For example, bacteremia and acute endocarditis are often caused by *Staphylococcus aureus* (*S. aureus*) [4,5]. Besides, this kind of bacteria can bring about a variety of skin and soft tissue infections, especially when the skin or mucosal barriers are damaged [6–9]. Clinically, antibiotics therapy is an effective method to prevent and treat bacterial infections [10,11]. However, drug-resistance occurs when bacteria develop the ability to defeat the employed medicines [12,13]. Nowadays, antibiotic resistance becomes one of the biggest threats to the health of human beings. Therefore, it is urgent to develop a novel drug-free strategy for rapid and safe sterilization.

Recently, photothermal therapy (PTT) is considered to be an effective treatment strategy for some diseases such as tumor and bacterial

infection, which was depended upon the local hyperthermia produced by some photothermal transducing agents (PTAs) under light irradiation [14–17]. Among multitudinous PTAs, near-infrared (NIR) light-absorbing agents are attracting considerable attention due to the unique advantages, including noninvasiveness, no tissue damage, short treatment time and noticeable therapeutic effect [18–24]. Although some NIR light-absorbing nanomaterials such as gold nanoparticles (NPs) [25], silver NPs [26], graphene oxide [27], and Prussian blue-based NPs [28], have been widely investigated for PTT applications, their relatively poor biodegradability and high cost are the obstacles for the future clinical applications.

Humic substances, naturally derived from the microbial biodegradation of animal and plant remains through complex natural reactions, are the major fraction of natural organics [29]. Since ancient times, HuA has been utilized to availably treat and prevent many diseases [30], especially gynecological, musculoskeletal and

E-mail addresses: Liuxiangmei1978@163.com (X. Liu), shuilinwu@tju.edu.cn (S. Wu).

d Department of Orthopaedics & Traumatology, Li Ka Shing Faculty of Medicine, The University of Hong Kong, Pokfulam, Hong Kong, China

<sup>\*</sup> Corresponding authors.

dermatological diseases, which proves the biosafety of HuA for biomedical applications. A recent study has reported that HuA has an excellent ability to convert NIR light energy into heat [31]. Therefore, this natural HuA is a promising photothermal biomaterial for PTT because of its low cost and excellent biocompatibility [32].

Temperatures over 60 °C or higher are typically required for single PTT to kill bacteria by denaturing protein under hyperthermia, but the high temperature or a long-time exposure to NIR light may cause thermal damage to surrounding normal tissues [33]. However, a lower temperature (e.g., 43 °C) is not sufficient to achieve effective sterilization within a short time [34]. Thus, synergistic strategies are demanded.

Some metallic elements like Cu, Fe, and Zn are the necessary elements for human health because they are involved in many physiological reactions, including cellular reactions when they are at normal levels [35]. Many studies have reported the inhibitory action of elevated concentration of  $\mathrm{Zn}^{2+}$  against bacteria [36–38]. The underlying antibacterial mechanism of  $\mathrm{Zn}^{2+}$  is to perturb homeostasis and enhance proton permeability into bacterial membranes, thus inhibiting glycolysis, glucosyltransferase production and polysaccharide synthesis in bacteria [39]. However, it often takes a long time for  $\mathrm{Zn}^{2+}$  to kill bacteria effectively, which may cause zinc resistance in bacteria [40]. Thus, using only  $\mathrm{Zn}^{2+}$  as an antibacterial strategy is insufficient to reach an ideal bactericidal effect. Hence, we hypothesize that the combination of  $\mathrm{Zn}^{2+}$  with PTT would achieve much better antibacterial efficacy than  $\mathrm{Zn}^{2+}$  or PTT alone through a synergistic action.

As organic-inorganic hybrid porous materials, metal-organic frameworks (MOFs) are composed of metal ions/clusters and organic ligands with a repeating cage-like structure [41,42], which endows MOFs with high specific surface area, tunable pore size, and theoretically infinite structures. As a result, MOFs have recently been widely utilized to develop novel functional materials [43,44]. As a representative of MOFs, zeolitic imidazolate framework (ZIF-8), has been investigated for plenty of biomedical applications due to its tunable functionalities and high porosity [45,46]. The recent study disclosed the NIR-induced dissociation phenomenon of ZIF-8 at pH 7.4 [47]. As a result, we can propose another hypothesis that it is feasible to control the release of Zn<sup>2+</sup> from ZIF-8 under NIR irradiation to help kill bacteria.

Given the above two assumptions, in this work, HuA was encapsulated in the MOF of ZIF-8 to form nanocomposites (HuA@ZIF-8 NPs), which was achieved by the in-situ growth of ZIF-8 around

polyvinylpyrrolidone (PVP)-modified HuA (Scheme 1). And the Zn<sup>2+</sup>-assisted photothermal therapy for rapid bacteria-killing was developed through NIR irradiation. The synergistic action was achieved by local hyperthermia produced by HuA and the controlled release of Zn<sup>2+</sup> from the composites under the irradiation, contributing to the excellent antibacterial efficiency of HuA@ZIF-8 within a short time, *i.e.* 99.59 % and 99.37 % against *Staphylococcus aureus* and *Escherichia coli* with 20 min NIR irradiation, respectively.

#### 2. Experimental procedures

## 2.1. Synthesis of PVP-modified humic acid

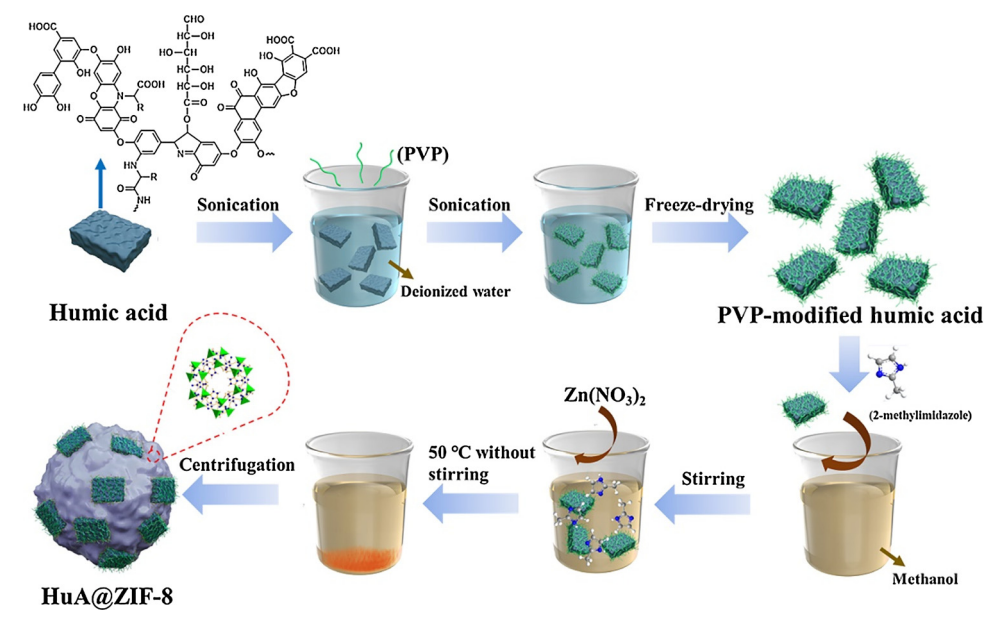
Firstly, 40 mg of humic acid (HuA) was added into 1.5 mL of deionized (DI) water, ultrasonically dispersed for 30 min to obtain a HuA colloidal solution, and then 80 mg of PVP was added to the above HuA colloidal solution. After that, the mixture was sonicated for 3 h. Finally, black PVP-modified HuA powders were obtained by freeze-drying the mixture.

#### 2.2. Fabrication of ZIF-8

Briefly, 4 mL of 2-methylimidazole methanol solution (8 mg/mL) and 4 mL of a  $\rm Zn(NO_3)_2$  methanol solution (27.5 mg/mL) were added to into 23 mL of methanol with continuous stirring. After stirring for 10 min, the reaction solution was left at 50 °C for 3 h without stirring. After the reaction, the as-prepared ZIF-8 was collected by the centrifugation at 12,000 rpm for 10 min, washed twice by methanol, and finally dried at 50 °C for 4 h for further use.

#### 2.3. Synthesis of HuA@ZIF-8 NPs

To fabricate the HuA@ZIF-8 NPs,  $4\,\text{mL}$  of 2-methylimidazole methanol solution (8 mg/mL) and 3 mL of PVP-modified HuA methanol solution (1 mg/mL) were simultaneously added into 20 mL of methanol. After stirring for  $10\,\text{min}$ ,  $4\,\text{mL}$  of a  $\text{Zn}(\text{NO}_3)_2$  methanol solution (27.5 mg/mL) was added into the above mixtures and stirred for another  $10\,\text{min}$ . Then, the mixtures were left at  $50\,^\circ\text{C}$  for  $3\,\text{h}$  without stirring. When the reaction was over, dark brown powders were observed to precipitate at the bottom of the solution, indicating the formation of HuA@ZIF-8 NPs. The supernatant was discarded out, and the



Scheme 1. Schematic illustration of the synthesis of the HuA@ZIF-8 NPs by in situ growth of ZIF-8 around PVP-modified HuA.

product was centrifuged at 9000 rpm for 10 min, then washed twice by methanol, dried at 50  $^{\circ}$ C for 4 h for further use.

#### 2.4. Materials characterization

The size and morphologies of the synthesized nano-powders were observed using scanning electron microscopy (SEM, JSM6510LV) equipped with energy-dispersive spectroscopy (EDS) and transmission electron microscopy (TEM, Tecnai G20, FEI, USA). The crystallinity and the purity of the NPs were examined by XRD (D8A25, BRUKER, Germany) using Cu K $\alpha$  radiation ( $\lambda=1.54051, 1.54433 \mbox{\normalfont A}$ ) over the 20 range of 5 - 30°. The chemical compositions of the materials were identified by a Fourier transform infrared spectroscopy (FTIR, NICOLET iS10) and X-ray photoelectron spectroscopy (XPS, ESCALAB 250Xi, Thermo Scientific, USA). The Vis–NIR spectra were determined using a UV–vis-NIR spectrometer (UV–vis-NIR, UV–3600, Shimadu, Japan).

#### 2.5. Photothermal performance test

The dispersions of the HuA@ZIF-8 NPs with four kinds of concentrations (0, 200, 500 and 1000  $\mu$ g/mL) in phosphate-buffered saline (PBS, pH = 7.4) were exposed to the 808 nm NIR laser (power density:  $1.8 \, \text{W/cm}^2$ ) for 20 min, and the Thermal Imager (FLIR, E40, with an accuracy of 0.1 °C) was utilized to monitor the temperature at 1 min intervals for a total of 20 min.

# 2.6. In vitro release of Zn2+

To measure the release of  $Zn^{2+}$  from HuA@ZIF-8 NPs under 808 nm irradiation,  $1000\,\mu\text{g/mL}$  of the HuA@ZIF-8 NPs dispersed in PBS were exposed to the 808 nm NIR laser for different periods of time up to 20 min and then centrifuged at 12,000 rpm for 10 min. The supernatant was collected and analyzed by inductive coupled plasma atomic emission spectrometry (ICP-AES, Optimal 8000, PE, USA) to determine the released concentration of  $Zn^{2+}$  from HuA@ZIF-8 NPs.

# 2.7. In vitro antibacterial test

In this work, the spread plate experiments were carried out to evaluate the antibacterial efficacy of the HuA@ZIF-8 NPs against *Escherichia coli (E. coli)* and *Staphylococcus aureus (S. aureus)* as the representative of Gram-negative bacteria and Gram-positive bacteria. According to the standard process, sterile Luria-Bertani (LB) broth and LB agar plates were prepared. Each group contained three parallel samples for the antibacterial test.  $20\,\mu\text{L}$  of four different concentration dispersions (0, 2, 5 and  $10\,\text{mg/mL}$ ) of the HuA@ZIF-8 NPs in PBS was added into 96-well plates containing  $180\,\mu\text{L}$  mixtures of diluted bacterial suspension ( $10^7$  CFU/mL) cultured in the sterile (LB) culture medium, respectively. All samples were divided into two groups, *i.e.*, one was irradiated with 808 nm NIR laser for 20 min and another was cultured without irradiation for 20 min.

After having been irradiated for 20 min or cultured without light for 20 min,  $20\,\mu\text{L}$  solution was extracted from each well and spread on the surface of LB agar plate after diluting. Then, the LB agar plates contained *E. coli* or *S. aureus* were incubated at 37 °C for 24 h. Afterwards, the bacterial colony on the plates was photographed, and the numbers of viable bacterial colony-forming units (CFUs) were counted, and the antibacterial ratio was calculated according to the previous study [43].

To further evaluate the antibacterial activity of the HuA@ZIF-8 NPs, Live/Dead fluorescence staining was used in this work. The details were referred to our previous publication [14].

#### 2.8. Cell culture

Mouse fibroblasts cells line (NIH3T3-E1) was applied in this work. They were cultured in MEM/EBSS (HyClone) medium supplemented

with 10 % fetal bovine serum (FBS), 1 % penicillin – streptomycin solution, and 1 % Amino Acids Solution, then incubated in a humidified atmosphere of 5 %  $\rm CO_2$  at 37 °C. The medium was refreshed every three days. The detailed procedure can be found in elsewhere [36,43].

#### 2.9. In vitro cytotoxicity assay

The cytotoxicity of the HuA@ZIF-8 NPs was tested by using a 3-(4.5-dimethylthiazol-2-yl)-2,5-diphenyltetrazolium bromide (MTT) assay of cellular activity on the NIH3T3-E1 cells. Before the assay, the NIH3T3-E1 cells ( $5\times10^4$  cells/cm²) were maintained in Dulbecco's modified eagle medium (DMEM), then seeded in 96-well plates (200 µL total volume per well) and cultured for 24 h. After the cell attached to the wall, four HuA@ZIF-8 NPs samples, which were diluted to 0, 200, 500, 1000 µg/mL in DMEM, were added to the well, respectively. Each sample was divided into two groups (irradiated with 808 nm NIR laser for 20 min or cultured without irradiation for 20 min).

After having been irradiated for 20 min or cultured without irradiation for 20 min, the cells were incubated for 8 h and 24 h, respectively. Afterwards, the MTT solution with a concentration of  $5\,\mu g/mL$  was added into each well and incubated for 4 h at 37 °C. After that, the medium was removed, 200  $\mu L$  dimethyl sulfoxide (DMSO) solution was added to each well, and the plate was shaken for 10 min. Afterwards, the solution was left standing for 12 h, 100  $\mu L$  of the supernatant was taken out and measured by a microplate reader (SpectraMax I3MD USA) to determine its absorbance (OD) at 490 nm [43,48]. The results were expressed as the percentage of cell viability, and the experiment was carried out in triplicate.

# 2.10. In vitro cell morphology

Following the MTT assay procedures above, the cells with a density of  $5\times10^4$  cells/cm² were co-cultured with different concentration dispersions of HuA@ZIF-8 NPs in a 96-well plate for 8 h and then rinsed three times with PBS. Next, the cells were fixed with 4 % paraformaldehyde solution at room temperature for 10 min and then rinsed with PBS. Subsequently, the cells were stained with Tetramethylrhodamine (TRICT) at room temperature for 30 min, rinsed with PBS, and then further stained with 4′, 6-diamidino 2-phenylindole (DAPI; YiSen, Shanghai) for 30 s. After washing with PBS for 2 times, the cell morphologies were observed by the inverted fluorescence microscope (IFM, Olympus, IX73).

## 2.11. Statistic analysis

To ensure the scientific and rigorous results of the experiment, all the experimental data were evaluated as mean  $\pm$  standard deviation based on at least three tests and analyzed by the one-way ANOVA.

#### 3. Results and discussion

# 3.1. Preparation and characterization of HuA@ZIF-8 NPs

As shown in Fig. 1a, the SEM image showed that the synthesized ZIF-8 NPs exhibited a nano-cube structure with a uniform size of about 500 nm. In contrast, the *in-situ* growth of ZIF-8 on the surface of polyvinylpyrrolidone (PVP)-modified HuA induced a significantly decreased size of the synthesized HuA@ZIF-8 NPs with an irregular shape. It was observed from Fig. 1b that the average size of HuA@ZIF-8 NPs was about 120 nm. In this work, PVP was absorbed by the surface of HuA colloidal particles to form PVP-modified HuA. According to the previous study, PVP adsorbed on nanoparticles surface played the role of stabilizing the nanoparticles in the reaction solution and enhancing the affinity of the nanoparticles to coordination-polymer spheres through weak coordination interactions between pyrrolidone rings (C=O) and zinc atoms in ZIF nodes and through hydrophobic interactions between

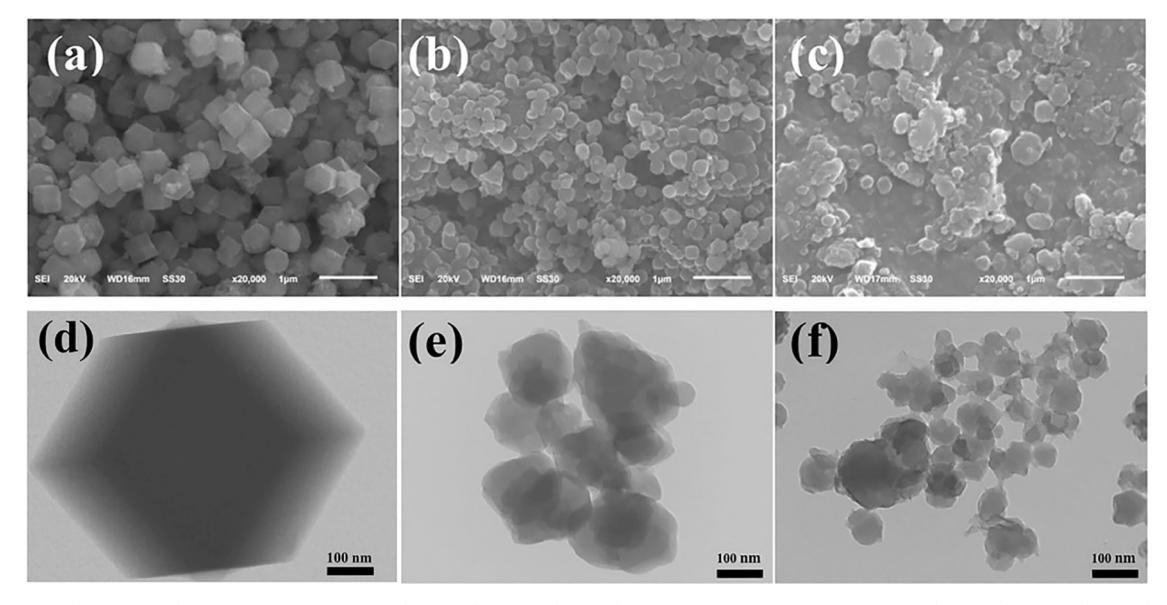


Fig. 1. SEM images of (a) ZIF-8, (b) HuA@ZIF-8 NPs exposed to NIR laser irradiation for 0 min, (c) HuA@ZIF-8 NPs exposed to NIR laser irradiation for 20 min; TEM images of (d) ZIF-8, (e) HuA@ZIF-8 NPs exposed to NIR laser irradiation for 0 min, (f) HuA@ZIF-8 NPs exposed to NIR laser irradiation for 20 min.

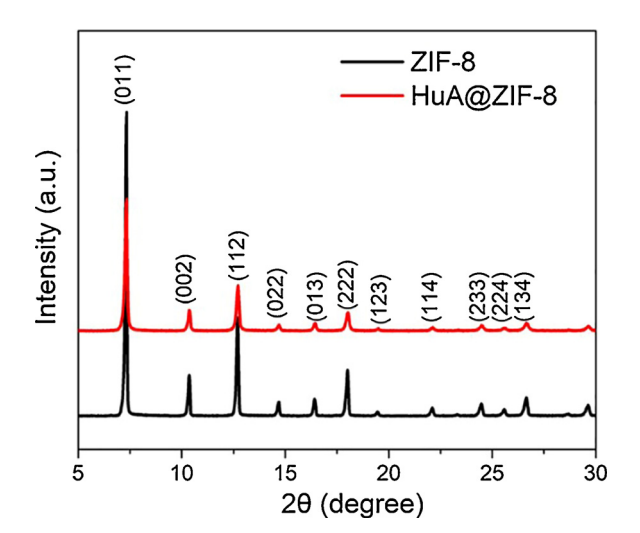


Fig. 2. XRD patterns of the synthesized nanoparticles.

apolar groups of PVP and organic linkers [49]. The above two interactions could account for the decreased size and irregular shape of HuA@ZIF-8 NPs compared with ZIF-8 NPs. In comparison with asprepared HuA@ZIF-8, the 20 min NIR laser irradiation induced the

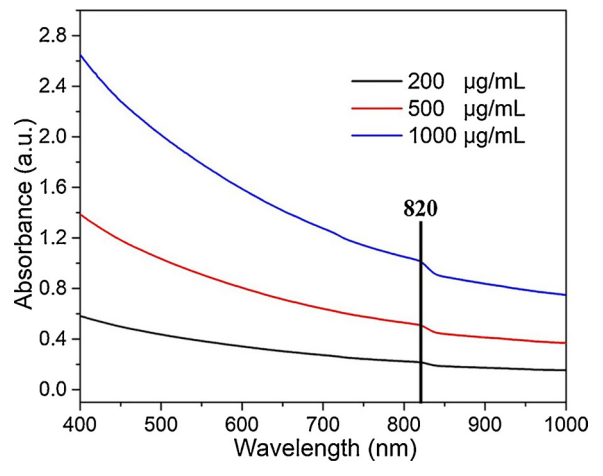


Fig. 4. Vis - NIR absorption spectra of prepared HuA@ZIF-8 NPs dispersions in PBS with different concentrations (Black straight line: the sharp decrease of light absorption at 820 nm).

significant change of composite NPs with more irregular shape and much smaller size of about  $40-100\,\mathrm{nm}$  (Fig. 1c), which might be due to that the photothermal effects of HuA induce the disintegration of the NPs. The TEM images shown in Fig. 1d-1f further disclosed the

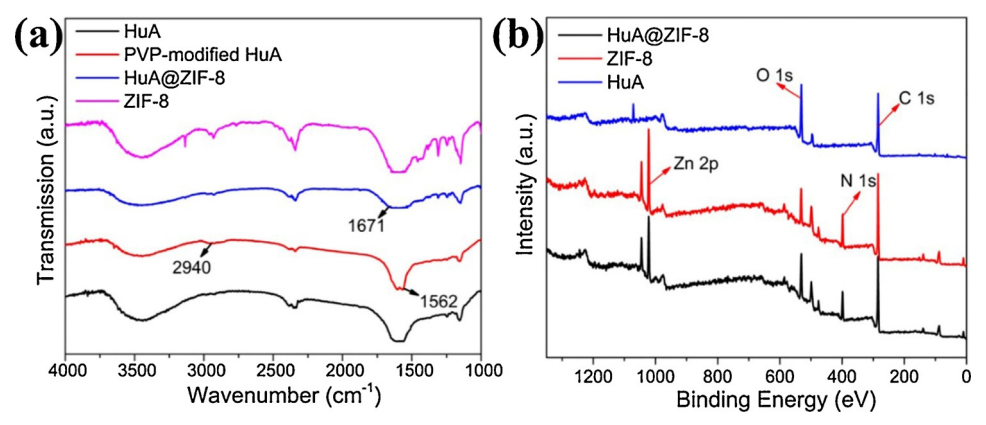


Fig. 3. Chemical compositions of synthesized materials. (a) FTIR spectra, (b) XPS survey scan.

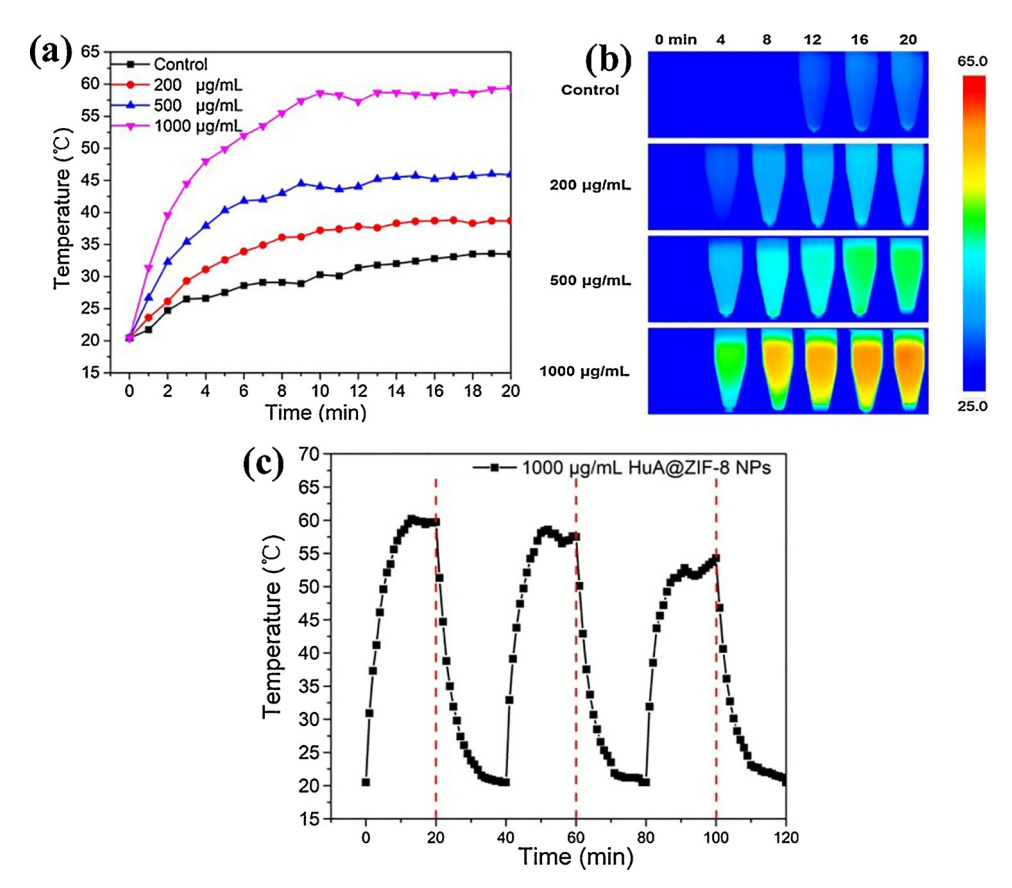


Fig. 5. Photothermal heating curves of the prepared HuA@ZIF-8 NPs dispersions in PBS with different concentrations (a), and the corresponding real-time infrared thermal images (b), and the cyclic photothermal heating curves of HuA@ZIF-8 NPs with a concentration of 1000 μg/mL (c).

evolution of corresponding NPs, which was in good agreement with the SEM observation.

As shown in Figure S1, the SEM images showed the morphologies of the HuA@ZIF-8 NPs in the same conditions as the cell culture (Petri dishes, cell culture medium, 37 °C, 5 % CO $_2$ , etc.) for 8 h and 24 h, respectively. Both Figure S1a and Figure S1b showed little change in the structure of the nanoparticles, indicating that HuA@ZIF-8 NPs might be relatively stable in the cell culture conditions.

The X-ray diffraction (XRD) patterns shown in Fig. 2 revealed the good crystallization of as-synthesized ZIF-8 and HuA@ZIF-8 NPs. In this work, our prepared ZIF-8 showed the peaks at 7.3°, 10.3°, 12.8°, 18.25°, corresponding to the crystal plane of (011), (002), (112), and (222), respectively, which was in accordance with the phase structure of standard ZIF-8 [49,50]. In addition, the as-prepared HuA@ZIF-8 NPs exhibited almost the same XRD pattern as the one of ZIF-8, indicating their same phase structure. However, compared with the XRD pattern obtained from the former, the full width at half maxima of the latter decreased significantly, indicating the intensive reduction of the particle size of the as-synthesized HuA@ZIF-8 NPs, which was in line with the results shown in Fig. 1.

As shown in Fig. 3a, the FTIR spectrum of the PVP-modified HuA displayed the peaks at 2940 cm<sup>-1</sup> and 1562 cm<sup>-1</sup>. The former was assigned to the C–H stretching bond vibration of PVP while the latter belonged to the radical of –COOH belonged to HuA [32], demonstrating the successful grafting of PVP with HuA. In comparison with ZIF-8, the new peak at 1671 cm<sup>-1</sup> in the FTIR spectrum obtained from HuA@ZIF-8 was assigned to the C=O stretching bond vibration of PVP in the humic acid, suggesting the successful encapsulation of HuA with ZIF-8. XPS survey scan shown in Fig. 3b disclosed that after encapsulation, the signal intensity of Zn and N in HuA@ZIF-8 decreased slightly compared with the one in ZIF-8. The signal of O1s was increased evidently (Table S1), further suggesting the capsulation of HuA

in the frameworks of ZIF-8. XPS narrow scan disclosed that except for intensity, the measured binding energy of Zn2p3 (Figure S2a) and N1s (Figure S2b) was the same in ZIF-8 and HuA@ZIF-8, indicating that the HuA encapsulation did not change the original chemical bonding of ZIF-8. However, both O1s (Figure S2c) and C1s (Figure S2d) narrow spectra in HuA@ZIF-8 showed wider peaks compared with the corresponding ones obtained from HuA and ZIF-8, further proving the successful combination of HuA in ZIF-8.

# 3.2. NIR controlled hyperthermia and $Zn^{2+}$ release

Fig. 4 showed the Vis - NIR absorption spectra of the HuA@ZIF-8 NPs dispersions with different concentrations. It was observed that the prepared HuA@ZIF-8 NPs dispersions in PBS exhibited a broad absorbance in the Vis-NIR region and the absorption ability decreased with the increased wavelength, which exhibited the similar trend with the reported results of sodium humate [31], further confirming the successful introduction of HuA in the HuA@ZIF-8 NPs. In addition, a sharp decrease of light absorption occurred at the wavelength of 820 nm, suggesting the reasonability to select 808 nm NIR light to inspire the photothermal effects of HuA@ZIF-8 NPs. It was evident that the NIR light absorption ability was gradually increased as the concentration of NPs increased. As shown in Fig. 5a, with NIR light irradiation, the temperatures of all the samples increased rapidly and reached a plateau after irradiation for 10 min. The maximal temperature of 0, 200, 500 and 1000 µg/mL dispersions of the HuA@ZIF-8 NPs in PBS was 33.6 °C, 38.7 °C, 45.9 °C, and 59.4 °C, respectively, indicating the concentrationdependent feature of photothermal performance of HuA@ZIF-8 NPs dispersions. Fig. 5b showed the corresponding real-time infrared thermal images of the HuA@ZIF-8 NPs dispersions with different concentrations, visually illustrating that HuA@ZIF-8 NPs performed good photothermal effects under the irradiation of NIR light. Fig. 5c showed

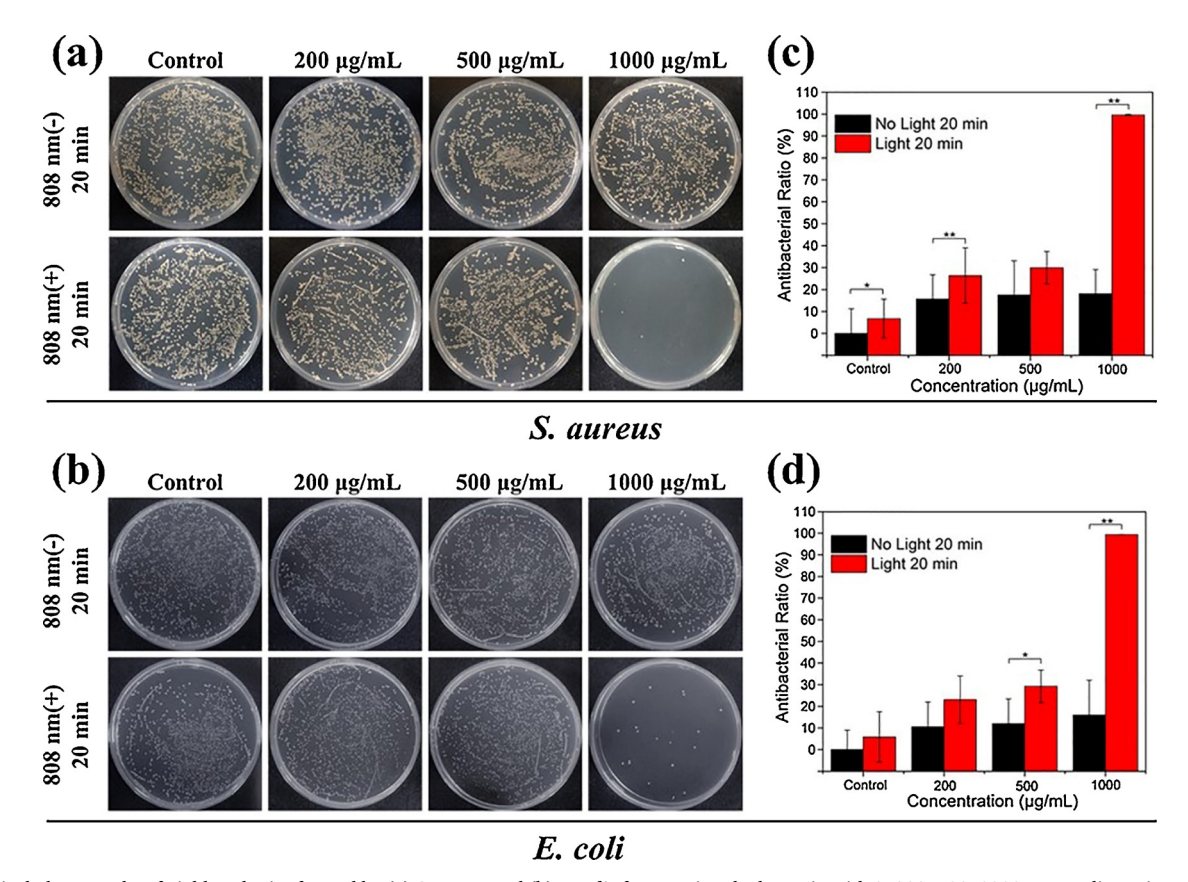


Fig. 6. Typical photographs of viable colonies formed by (a) *S. aureus* and (b) *E. coli* after treating the bacteria with 0, 200, 500, 1000  $\mu$ g/mL dispersions of the HuA@ ZIF-8 NPs with or without 808 nm NIR laser irradiation for 20 min. The corresponding histograms of the antibacterial ability towards (c) *S. aureus* and (d) *E. coli* obtained from the spread plate results are presented as the mean  $\pm$  standard deviations: \*P < 0.05, \*\*P < 0.01 and\*\*\*P < 0.001, n = 3.

the cyclic photothermal heating curves of HuA@ZIF-8 NPs with a concentration of  $1000\,\mu g/mL$ . It was evident that as the cyclic number of irradiation increased, the temperature decreased slightly. After 3 cycles, the temperature decreased from 59.4 °C to 54 °C, which was ascribed to the local pyrolysis of HuA@ZIF-8 NPs shown in Fig. 1.

As measured by inductive coupled plasma atomic emission spectrometry (ICP-AES) (Figure S3), the Zn2+ release concentration from the HuA@ZIF-8 NPs was increased as the irradiation time increased. After being irradiated by 808 nm NIR light for 5, 10, 15 and 20 min, the Zn<sup>2+</sup> release concentration of 1000 μg/mL HuA@ZIF-8 NPs dispersion was 1.36, 1.74, 2.03 and 2.53 mg/L, respectively. The maximum Zn<sup>2+</sup> concentration was much lower than 6.0 mg/L, which was reported to be the threshold value of cytotoxicity in vitro [51]. As contrast, very few Zn<sup>2+</sup> ions were released from the group of 1000 µg/mL HuA@ZIF-8 NPs immersed in PBS within 20 min in the dark. These results indicated that the controlled release of  $\mathrm{Zn}^{2+}$  could be achieved through NIR irradiation for different time. This was due to the fact that the as-synthesized HuA@ZIF-8 NPs kept intact while local hyperthermia produced by NIR irradiation made the composites disintegration gradually as the irradiation time increased, which accelerated the leaching of Zn2+ from HuA@ZIF-8 NPs.

# 3.3. Antibacterial activity in vitro

The antibacterial activity of the HuA@ZIF-8 NPs against *S. aureus* and *E. coli* was evaluated by the spread plate method. In this work, the HuA@ZIF-8 NPs were observed to exhibit similar antibacterial trend against both *S. aureus* and *E. coli*. Compared with the groups without irradiation, the corresponding NIR irradiated group showed enhanced antibacterial efficacy against *S. aureus* (Fig. 6a) and *E. coli* (Fig. 6b). With the increase of concentration of HuA@ZIF-8 NPs, after being

exposed to the 808 nm NIR laser for 20 min, the antibacterial efficacy of HuA@ZIF-8 NPs with 0, 200, 500 and 1000 μg/mL were calculated to be 6.74 %, 26.33 %, 29.91 %, and 99.59 % against S. aureus (Fig. 6c) and 5.84 %, 23.10 %, 29.26 %, and 99.37 % against E. coli (Fig. 6d), respectively. These results suggested the concentration-dependent feature of the antibacterial activity of HuA@ZIF-8 NPs. 1000 µg/mL of HuA@ZIF-8 NPs achieved the highest antibacterial efficacy among them because the highest temperature and the largest amount of released Zn2+ were achieved at this concentration according to the results shown in Fig. 5 and Figure S3. According to the previous literatures [33,34,40,52], single PTT with safe temperature or Zn<sup>2+</sup> with non-toxic concentration for normal tissues was not enough to kill bacteria effectively. This is why even the group with 1000 µg/mL HuA@ ZIF-8 NPs exhibited a lower antibacterial ratio below 20 % towards two types of bacteria after culturing for 20 min in the dark. Live/dead fluorescence staining of bacteria co-cultured with different samples was performed to demonstrate the antibacterial activity of the as-prepared HuA@ZIF-8 NPs further. The live bacteria were labelled with green fluorescence, while the dead bacteria were labelled with visible red fluorescence. As shown in Figure S4, both S. aureus and E. coli exhibited a similar trend for all groups. After being irradiated by 808 nm NIR light for 20 min, the red spots on those groups were obviously increased with increasing concentration of HuA@ZIF-8 NPs, indicating that the increased concentration enhanced the ability of HuA@ZIF-8 NPs to kill bacteria, which was in accordance with the spread plate results. Conversely, the red spots of all groups without irradiation were negligible, revealing the relatively poor antibacterial ability of the samples without irradiation.

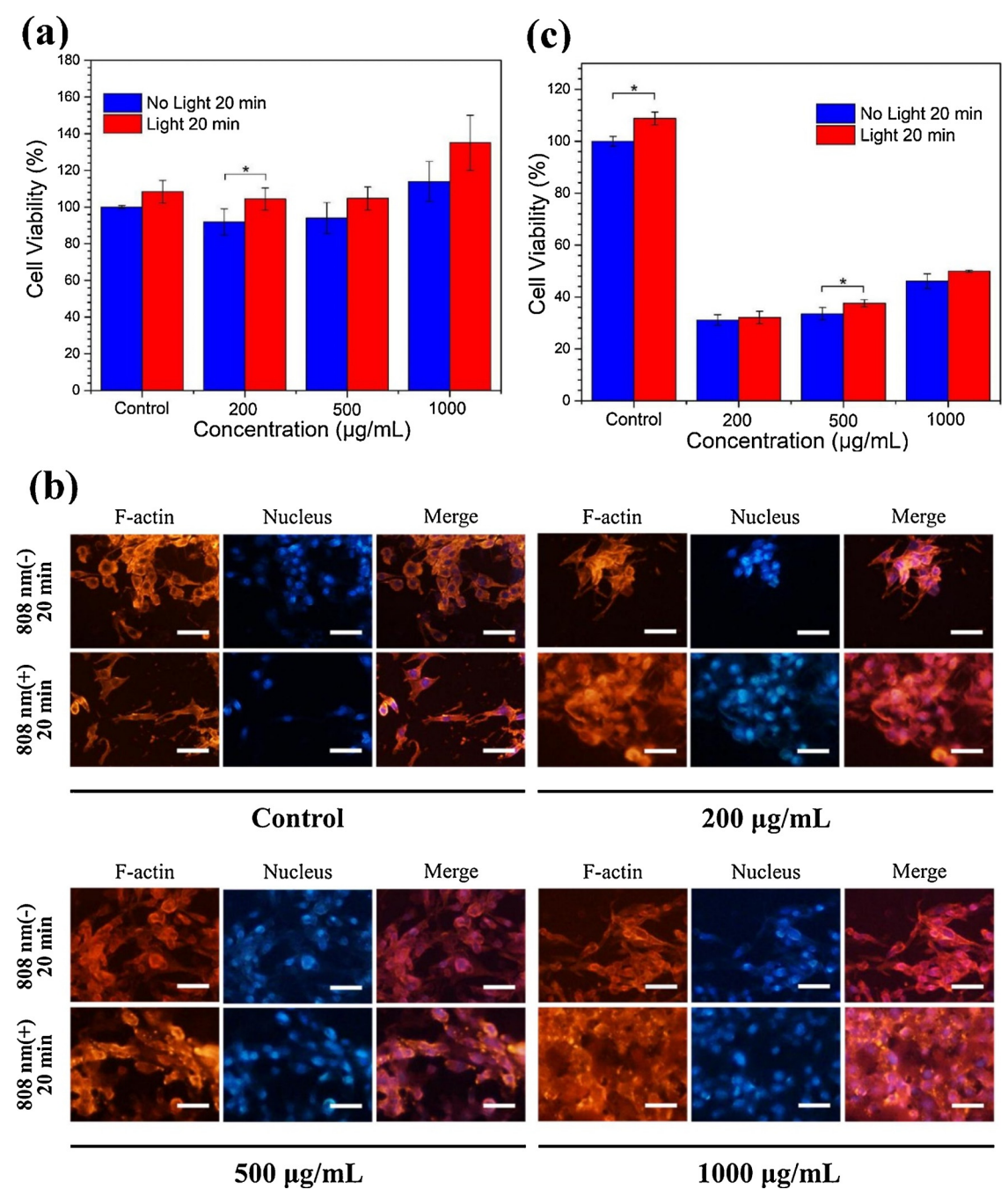


Fig. 7. In vitro cytotoxicity results and cell morphology. Cell viability after co-treatment with 0, 200, 500,  $1000\,\mu g/mL$  dispersions of the HuA@ZIF-8 NPs with or without 808 nm NIR laser irradiation for 20 min and co-culture for 8 h (\*P < 0.05, \*\*P < 0.01, \*\*\*P < 0.001, n = 3) (a), and the corresponding cell fluorescence staining photographs (b), the orange color indicates F-actin, and the blue color indicates nuclei (scar bar:  $50\,\mu m$ ). And the MTT assay of cell viability after co-treatment and co-culture for  $24\,h$  (\*P < 0.05, \*\*P < 0.01, \*\*\*P < 0.001, n = 3) (c) (For interpretation of the references to colour in this figure legend, the reader is referred to the web version of this article).

# 3.4. In vitro cytotoxicity

The evaluation of the biocompatibility of the HuA@ZIF-8 NPs measured by MTT was shown in Fig. 7a. After the treatments of the HuA@ZIF-8 NPs dispersions under 808 nm NIR laser irradiation for 20 min and the followed co-culturing for 8 h, NIH3T3-E1 cell viability in 0, 200, 500 and 1000  $\mu$ g/mL of HuA@ZIF-8 NPs were calculated to be 108.37 %, 104.38 %, 104.69 %, and 135.04792 % respectively. As for the group without laser irradiation, no apparent change on cell viability was observed. Both Vis — NIR absorbance spectra of the nanocomposites after 24 h incubated in cell culture conditions (without

cells) and in PBS were performed in a wavelength range including 490 nm (Figure S5), and it seemed that the remaining nanocomposites did not cause a significant impact on the MTT experiments. The cell morphology and spreading behaviors was examined, and the corresponding fluorescence images were shown in Fig. 7b. After the treatments of the HuA@ZIF-8 NPs dispersions under 808 nm NIR laser irradiation for 20 min and co-culture for 8 h, there was no apparent change of morphology in 0, 200, 500 and  $1000\,\mu\text{g/mL}$  of HuA@ZIF-8 groups. For short exposition times, the nanocomposites did not seem to be cytotoxic, even though more studies should be performed.

Nevertheless, as shown in Fig. 7c, the cell viability decreased

sharply after the treatments with 200, 500,  $1000 \,\mu g/mL$  dispersions of the HuA@ZIF-8 NPs and co-culture for 24 h, no matter with or without NIR laser irradiation, indicating that a long time co-culture with HuA@ZIF-8 NPs could be adverse to the cell viability. Thus, it is necessary to control the contact time of cells with HuA@ZIF-8 NPs to avoid toxicity in the practical application.

#### 4. Conclusion

In summary, HuA encapsulated ZIF-8 (HuA@ZIF-8) nanocomposites have been successfully fabricated by the in-situ growth of ZIF-8 around PVP-modified HuA. The NIR light was not only absorbed by the HuA in composites to convert into heat, but also controlled the release of  $Zn^{2+}$ from ZIF-8 along with the dissociation of composites. The HuA@ZIF-8 NPs possessed the concentration-dependent property of photothermal performance, and the concentration of controlled release of Zn<sup>2+</sup> was increased with the prolonged irradiation time. The combination of Zn<sup>2+</sup> and PTT achieved a rapid and effective sterilization. Besides, the NIR irradiated groups showed enhanced antibacterial efficiency in comparison with the groups without being irradiated, and the antibacterial activity of HuA@ZIF-8 NPs was proven to be concentrationdependent. In addition, HuA@ZIF-8 NPs did not seem to be cytotoxic in short exposition times. Thus, in consideration of the superiorities of NIR-induced PTT, excellent antibacterial efficiency, good biodegradability, and low cost, this light-responsive platform can be promising for public health applications, including bacterial infection.

## CRediT authorship contribution statement

Ziwei Liu: Conceptualization, Methodology, Data curation, Writing - original draft. Lei Tan: Methodology, Data curation, Writing - original draft, Project administration. Xiangmei Liu: Conceptualization, Writing - review & editing, Supervision, Project administration. Yanqin Liang: Methodology. Yufeng Zheng: Visualization, Writing - review & editing. Kelvin Wai Kwok Yeung: Writing - review & editing. Zhenduo Cui: Visualization, Writing - review & editing. Shengli Zhu: Methodology. Zhaoyang Li: Methodology. Shuilin Wu: Conceptualization, Writing - review & editing, Supervision, Project administration.

#### **Declaration of Competing Interest**

The authors declare that they have no known competing financial interests or personal relationships that could have appeared to influence the work reported in this paper.

### Acknowledgements

This work is jointly supported by the Natural Science Fund of Hubei Province, 2018CFA064, National Natural Science Foundation of China, Nos. 51671081, 51871162, 51801056 and National Outstanding Youth Science Fund Project of NSFC51925104, and Hong Kong ITC (ITS/287/17, GHX/002/14SZ), Health and Medical Research Fund (03142446), as well as Hong Kong RGC GRF (17214516) and RGC/NSFC (N HKU725-16).

# Appendix A. Supplementary data

Supplementary material related to this article can be found, in the online version, at doi:https://doi.org/10.1016/j.colsurfb.2020.110781.

# References

- [1] M.J. Pallen, B.W. Wren, Bacterial pathogenomics, Nature 449 (2007) 835–842.
- [2] G.J. Chan, A.C.C. Lee, A.H. Baqui, J.W. Tan, R.E. Black, Risk of early-onset neonatal infection with maternal infection or colonization: a global systematic review and

- eeta-analysis, PLoS Med. 10 (2013) 20.
- [3] J.M. Sweere, J.D. Van Belleghem, H. Ishak, M.S. Bach, M. Popescu, V. Sunkari, G. Kaber, R. Manasherob, G.A. Suh, X. Cao, C.R. de Vries, D.N. Lam, P.L. Marshall, M. Birukova, E. Katznelson, D.V. Lazzareschi, S. Balaji, S.G. Keswani, T.R. Hawn, P.R. Secor, P.L. Bollyky, Bacteriophage trigger antiviral immunity and prevent clearance of bacterial infection, Science 363 (2019) eaat9691.
- [4] S.Y.C. Tong, J.S. Davis, E. Eichenberger, T.L. Holland, V.G. Fowler, Staphylococcus aureus infections: epidemiology, pathophysiology, clinical manifestations, and management, Clin. Microbiol. Rev. 28 (2015) 603–661.
- [5] P. Panizzi, M. Nahrendorf, J.L. Figueiredo, J. Panizzi, B. Marinelli, Y. Iwamoto, E. Keliher, A.A. Maddur, P. Waterman, H.K. Kroh, F. Leuschner, E. Aikawa, F.K. Swirski, M.J. Pittet, T.M. Hackeng, P. Fuentes-Prior, O. Schneewind, P.E. Bock, R. Weissleder, In vivo detection of Staphylococcus aureus endocarditis by targeting pathogen-specific prothrombin activation, Nat. Med. 17 (2011) 1142–U1153.
- [6] D.J. Tobin, Biochemistry of human skin our brain on the outside, Chem. Soc. Rev. 35 (2006) 52–67.
- [7] A. Abtin, R. Jain, A.J. Mitchell, B. Roediger, A.J. Brzoska, S. Tikoo, Q. Cheng, L.G. Ng, L.L. Cavanagh, U.H. von Andrian, M.J. Hickey, N. Firth, W. Weninger, Perivascular macrophages mediate neutrophil recruitment during bacterial skin infection, Nat. Immunol. 15 (2014) 45–53.
- [8] D. Parker, P.J. Planet, G. Soong, A. Narechania, A. Prince, Induction of type I interferon signaling determines the relative pathogenicity of staphylococcus aureus strains, PLoS Pathog. 10 (2014) 12.
- [9] L.M. Schlecht, B.M. Peters, B.P. Krom, J.A. Freiberg, G.M. Haensch, S.G. Filler, M.A. Jabra-Rizk, M.E. Shirtliff, Systemic staphylococcus aureus infection mediated by candida albicans hyphal invasion of mucosal tissue, Microbiology 161 (2015) 168–181
- [10] M. Baym, T.D. Lieberman, E.D. Kelsic, R. Chait, R. Gross, I. Yelin, R. Kishony, Spatiotemporal microbial evolution on antibiotic landscapes, Science 353 (2016) 1147–1151.
- [11] M.A. Fischbach, C.T. Walsh, Antibiotics for emerging pathogens, Science 325 (2009) 1089–1093.
- [12] Y. Liu, H.J. Busscher, B.R. Zhao, Y.F. Li, Z.K. Zhang, H.C. van der Mei, Y.J. Ren, L.Q. Shi, Surface-adaptive, antimicrobially loaded, micellar nanocarriers with enhanced penetration and killing efficiency in staphylococcal biofilms, ACS Nano 10 (2016) 4779–4789.
- [13] S.H. MacVane, Antimicrobial resistance in the intensive care unit: a focus on gramnegative bacterial infections, J. Intensive Care Med. 32 (2017) 25–37.
- [14] C.Y. Mao, Y.M. Xiang, X.M. Liu, Y.F. Zheng, K.W.K. Yeung, Z.D. Cui, X.J. Yang, Z.Y. Li, Y.Q. Liang, S.L. Zhu, S.L. Wu, Local photothermal/photodynamic synergistic therapy by disrupting bacterial membrane to accelerate reactive oxygen species permeation and protein leakage, ACS Appl. Mater. Interfaces 11 (2019) 17902–17914.
- [15] T.F. Tian, X.Z. Shi, L. Cheng, Y.C. Luo, Z.L. Dong, H. Gong, L.G. Xu, Z.T. Zhong, R. Peng, Z. Liu, Graphene-based nanocomposite as an effective, multifunctional, and recyclable antibacterial agent, ACS Appl. Mater. Interfaces 6 (2014) 8542–8548.
- [16] A. Chae, S. Jo, Y. Choi, B. Ryu, C.A. Choi, S.Y. Park, I. In, Enhanced photothermal bactericidal activity of chemically reduced graphene oxide stabilized by tripodal amphiphile, Appl. Surf. Sci. 474 (2019) 111–117.
- [17] M. Huo, L. Wang, H. Zhang, L. Zhang, Y. Chen, J. Shi, Construction of single-iron-Atom nanocatalysts for highly efficient catalytic antibiotics, Small (2019) e1901834
- [18] G.Y. Liu, J.H. Zou, Q.Y. Tang, X.Y. Yang, Y.W. Zhang, Q. Zhang, W. Huang, P. Chen, J.J. Shao, X.C. Dong, Surface modified Ti<sub>3</sub>C<sub>2</sub> MXene nanosheets for tumor targeting photothermal/photodynamic/chemo synergistic therapy, ACS Appl. Mater. Interfaces 9 (2017) 40077–40086.
- [19] R.F. Zhang, F. Yan, Y. Chen, Exogenous physical irradiation on titania semiconductors: materials chemistry and tumor-specific nanomedicine, Adv. Sci. 5 (2018) 28.
- [20] D.L. Han, Y.J. Han, J. Li, X.M. Liu, K.W.K. Yeung, Y.F. Zheng, Z.D. Cui, X.J. Yang, Y.Q. Liang, Z.Y. Li, S.L. Zhu, X.B. Yuan, X.B. Feng, C. Yang, S.L. Wu, Enhanced photocatalytic activity and photothermal effects of cu-doped metal-organic frameworks for rapid treatment of bacteria-infected wounds, Appl. Catal. B Environ. 261 (2020) 118248.
- [21] Z.M. Tang, P.R. Zhao, D.L. Ni, Y.Y. Liu, M. Zhang, H. Wang, H. Zhang, H.B. Gao, Z.W. Yao, W.B. Bu, Pyroelectric nanoplatform for NIR-II-triggered photothermal therapy with simultaneous pyroelectric dynamic therapy, Mater. Horizons 5 (2018) 946–952
- [22] T. Wei, Q. Yu, H. Chen, Responsive and Synergistic Antibacterial Coatings: Fighting against Bacteria in a Smart and Effective Way, Adv. Healthc. Mater. 8 (2019) 24.
- [23] Y.C. Qu, T. Wei, J. Zhao, S.B. Jiang, P. Yang, Q. Yu, H. Chen, Regenerable smart antibacterial surfaces: full removal of killed bacteria via a sequential degradable layer, J. Mater. Chem. B6 (2018) 3946–3955.
- [24] Y.H. Feng, L. Liu, J. Zhang, H. Aslan, M.D. Dong, Photoactive antimicrobial nanomaterials, J. Mater. Chem. B Mater. Biol. Med. 5 (2017) 8631–8652.
- [25] M.A. Huergo, L.J. Giovanetti, A.A. Rubert, C.A. Grillo, M.S. Moreno, F.G. Requejo, R.C. Salvarezza, C. Vericat, The surface chemistry of near-infrared resonant gold nanotriangles obtained via thiosulfate synthesis, Appl. Surf. Sci. 464 (2019) 131-130
- [26] Y. Qiao, F. Ma, C. Liu, B. Zhou, Q.L. Wei, W.L. Li, D.N. Zhong, Y.Y. Li, M. Zhou, Near-infrared laser-excited nanoparticles to eradicate multidrug-resistant bacteria and promote wound healing, ACS Appl. Mater. Interfaces 10 (2018) 193–206.
- [27] X. Ran, Y. Du, Z.Z. Wang, H. Wang, F. Pu, J.S. Ren, X.G. Qu, Hyaluronic acid-templated Ag nanoparticles/graphene oxide composites for synergistic therapy of bacteria infection, ACS Appl. Mater. Interfaces 9 (2017) 19717–19724.

- [28] S. Cai, J. Qian, S. Yang, L. Kuang, D. Hua, Acetylcysteine-decorated Prussian blue nanoparticles for strong photothermal sterilization and focal infection treatment, Colloids Surf. B Biointerfaces 181 (2019) 31–38.
- [29] M.N. Jones, N.D. Bryan, Colloidal properties of humic substances, Adv. Colloid Interface Sci. 78 (1998) 1–48.
- [30] R. Klöcking, B. Helbig, Medical Aspects and Applications of Humic Substances, Biopolymers for Medical and Pharmaceutical Applications, WILEY-VCH Verlag GmbH & C. KGaA, Weinheim. Germany, 2005, pp. 3–16.
- [31] Z.H. Miao, K. Li, P.Y. Liu, Z.L. Li, H.J. Yang, Q.L. Zhao, M.L. Chang, Q.Z. Yang, L. Zhen, C.Y. Xu, Natural humic-acid-based phototheranostic agent, Adv. Healthcare Mater. 7 (2018) 9.
- [32] M.M. Hou, R.H. Yang, L. Zhang, L.Y. Zhang, G. Liu, Z.G. Xu, Y.J. Kang, P. Xue, Injectable and natural humic acid/agarose hybrid hydrogel for localized lightdriven photothermal ablation and chemotherapy of cancer, ACS Biomater. Sci. Eng. 4 (2018) 4266–4277.
- [33] X.H. Wang, K. Su, L. Tan, X.M. Liu, Z.D. Cui, D.D. Jing, X.J. Yang, Y.Q. Liang, Z.Y. Li, S.L. Zhu, K.W.K. Yeung, D. Zheng, S.L. Wu, Rapid and highly effective noninvasive disinfection by hybrid Ag/CS@MnO₂ nanosheets using near-infrared light, ACS Appl. Mater. Interfaces 11 (2019) 15014–15027.
- [34] Y.J. Zhang, X.L. Zhan, J. Xiong, S.S. Peng, W. Huang, R. Joshi, Y. Cai, Y.L. Liu, R. Li, K. Yuan, N.J. Zhou, W.P. Min, Temperature-dependent cell death spectras induced by functionalized gold nanoparticle photothermal therapy in melanoma cells, Sci. Rep. 8 (2018) 9.
- [35] S. Parveen, R. Taranum, S. Mittapally, Metal ions as antibacterial agents, JDDT 8 (2018) 411–419.
- [36] Y.M. Xiang, C.Y. Mao, X.M. Liu, Z.D. Cui, D.D. Jing, X.J. Yang, Y.Q. Liang, Z.Y. Li, S.L. Zhu, Y.F. Zheng, K.W.K. Yeung, D. Zheng, X.B. Wang, S.L. Wu, Rapid and superior bacteria killing of carbon quantum dots/ZnO decorated injectable folic acidconjugated PDA hydrogel through dual-light triggered ROS and membrane permeability, Small 15 (2019) 15.
- [37] M.L. Kaariainen, C.K. Weiss, S. Ritz, S. Putz, D.C. Cameron, V. Mailander, K. Landfester, Zinc release from atomic layer deposited zinc oxide thin films and its antibacterial effect on Escherichia coli, Appl. Surf. Sci. 287 (2013) 375–380.
- [38] A. Wajda, W.H. Goldmann, R. Detsch, A.R. Boccaccini, M. Sitarz, Influence of zinc ions on structure, bioactivity, biocompatibility and antibacterial potential of meltderived and gel-derived glasses from CaO-SiO<sub>2</sub> system, J. Non-Cryst. Solids 511 (2019) 86–99.
- [39] T.N. Phan, T. Buckner, J. Sheng, J.D. Baldeck, R.E. Marquis, Physiologic actions of zinc related to inhibition of acid and alkali production by oral streptococci in suspensions and biofilms, Oral Microbiol. Immunol. 19 (2004) 31–38.
- [40] D.H. Nies, Microbial heavy-metal resistance, Appl. Microbiol. Biotechnol. 51 (1999)

- 730-750.
- [41] G. Ferey, Hybrid porous solids: past, present, future, Chem. Soc. Rev. 37 (2008) 191–214.
- [42] O.M. Yaghi, M. O'Keeffe, N.W. Ockwig, H.K. Chae, M. Eddaoudi, J. Kim, Reticular synthesis and the design of new materials, Nature 423 (2003) 705–714.
- [43] S. Lin, X.M. Liu, L. Tan, Z.D. Cui, X.J. Yang, K.W.K. Yeung, H.B. Pan, S.L. Wu, Porous iron-carboxylate metal-organic framework: a novel bioplatform with sustained antibacterial efficacy and nontoxicity, ACS Appl. Mater. Interfaces 9 (2017) 19248–19257.
- [44] Y.Y. Li, Y. Fang, Z.L. Cao, N.J. Li, D.Y. Chen, Q.F. Xu, J.M. Lu, Construction of g-C<sub>3</sub>N<sub>4</sub>/PDI@MOF heterojunctions for the highly efficient visible light-driven degradation of pharmaceutical and phenolic micropollutants, Appl. Catal. B Environ. 250 (2019) 150–162.
- [45] J. Zhuang, C.H. Kuo, L.Y. Chou, D.Y. Liu, E. Weerapana, C.K. Tsung, Optimized metal-organic-framework nanospheres for drug delivery: evaluation of small-molecule encapsulation, ACS Nano 8 (2014) 2812–2819.
- [46] P. Li, J.Z. Li, X. Feng, J. Li, Y.C. Hao, J.W. Zhang, H. Wang, A.X. Yin, J.W. Zhou, X.J. Ma, B. Wang, Metal-organic frameworks with photocatalytic bactericidal activity for integrated air cleaning, Nat. Commun. 10 (2019) 10.
- [47] Z.F. Wang, X.J. Tang, X.X. Wang, D.D. Yang, C. Yang, Y.B. Lou, J.X. Chen, N.Y. He, Near-infrared light-induced dissociation of zeolitic imidazole framework-8 (ZIF-8) with encapsulated CuS nanoparticles and their application as a therapeutic nanoplatform, Chem. Commun. 52 (2016) 12210–12213.
- [48] Y. Luo, J. Li, X.M. Liu, L. Tan, Z.D. Cui, X.B. Feng, X.J. Yang, Y.Q. Liang, Z.Y. Li, S.L. Zhu, Y.F. Zheng, K.W.K. Yeung, C. Yang, X.B. Wang, S.L. Wu, Dual metal-organic framework heterointerface, ACS Cent. Sci. 5 (2019) 1591–1601.
- [49] G. Lu, S.Z. Li, Z. Guo, O.K. Farha, B.G. Hauser, X.Y. Qi, Y. Wang, X. Wang, S.Y. Han, X.G. Liu, J.S. DuChene, H. Zhang, Q.C. Zhang, X.D. Chen, J. Ma, S.C.J. Loo, W.D. Wei, Y.H. Yang, J.T. Hupp, F.W. Huo, Imparting functionality to a metalorganic framework material by controlled nanoparticle encapsulation, Nat. Chem. 4 (2012) 310–316.
- [50] K.S. Park, Z. Ni, A.P. Cote, J.Y. Choi, R.D. Huang, F.J. Uribe-Romo, H.K. Chae, M. O'Keeffe, O.M. Yaghi, Exceptional chemical and thermal stability of zeolitic imidazolate frameworks, Proc. Natl. Acad. Sci. U. S. A. 103 (2006) 10186–10191.
- [51] A. Yamamoto, R. Honma, M. Sumita, Cytotoxicity evaluation of 43 metal salts using murine fibroblasts and osteoblastic cells, J. Biomed. Mater. Res. 39 (1998) 331–340.
- [52] J. Li, X.M. Liu, L. Tan, Z.D. Cui, X.J. Yang, Y.Q. Liang, Z.Y. Li, S.L. Zhu, Y.F. Zheng, K.W.K. Yeung, X.B. Wang, S.L. Wu, Zinc-doped Prussian blue enhances photothermal clearance of Staphylococcus aureus and promotes tissue repair in infected wounds. Nat. Commun. 10 (2019) 15.